Resonance scattering of sunlight by modulation of temporal coherence in microscale water aerosol

Stoyan P Penchev

AGU PUBLICATIONS

Geophysical Research Letters

RESEARCH LETTER
10.1002/2014GL059650

Resonance scattering of sunlight by modulation of temporal coherence in microscale water aerosol

Stoyan Penchev[1]

[1]Emil Djakov Institute of Electronics, Bulgarian Academy of Sciences, Sofia, Bulgaria

Abstract Resonance scattering of sunlight is an effect deduced from a rare atmospheric phenomenon known as solar glory. Its impressive spectral appearance is established by optical interference at precise modulation of the temporal coherence of sunlight within delaylines of microscale water droplets confined by refractive index. A ray-tracing method is used in the study correlated with analysis of the simulated convolution spectrum of backscatter pattern. Resonance modes of low finesse are formed on spectrally isolated intracavity optical paths preventing their destructive interference. The relevant modal wavelengths and diffraction angles are derived for selected temperature and droplet size. Simultaneously, the model explains the alternating polarization of the successive diffraction series.

The author is also Master of physics from St. Kliment Ohridski University in Sofia, Bulgaria, Doctor of physics and mathematics from A. M. Prohorov General Physics Institute, Moscow, associate researcher with the Institute of Physical and Chemical Research, RIKEN, Japan, bilateral research fellow of Bulgarian and Japanese ministries of education, laureate of the institutional Academician Djakov Award for achievements in science, with expertise in theoretical solid state physics, laser physics and spectroscopy, laser photothermal techniques for material science, and lidar remote sensing.

Key Points:
- Phenomenon of solar glory interpreted as resonance scattering of sunlight
- Optical interference inside delaylines of colliding microscale water droplets
- Resonance-established wavelengths at selected temperature and spherical size

Correspondence to:
S. Penchev,
penchev@bas.bg

Citation:
Penchev, S. (2014), Resonance scattering of sunlight by modulation of temporal coherence in microscale water aerosol, *Geophys. Res. Lett.*, *41*, doi:10.1002/2014GL059650.

Received 17 FEB 2014
Accepted 2 APR 2014
Accepted article online 11 APR 2014

1. Introduction

Solar glory is a phenomenon of the Earth's atmosphere observed strictly in anti-solar point of view as intense backscatter light of characteristic multi-color concentric rings. Its polarization is unusual with a central maximum of tangential polarization alternatively changing to radial for the outer rings. Its extraordinary appearance is worshiped in many cultures, and the Nobel Laureate Charles Thomson Rees Wilson tried to simulate the effect in laboratory. The conventional hypothesis based on calculations employs Mie-scattering model of a single spherical droplet (see, e.g., [*Laven,* 2005; http://www.philiplaven.com/p2c1a.html]). Despite the well-developed mathematical formalism, it is unable to explain the specular character of the glory without violation of certain principles of refraction and reflection expressed by geometric optics. A basic uncertainty comes from the assumption of a special, otherwise unobserved optical surface wave generated by some extraordinary conditions. It was introduced by Dutch astronomer Hendrik Christoffel van de Hulst in 1947 using a state-of-the-art analogy with electromagnetic microwaves propagating in the ground surface layer.

The spectral properties and specific atmospheric conditions of formation of solar glory are still a challenge to atmospheric optics. The paper brings forth a new concept of the phenomenon as an exceptional manifestation of the coherence properties of sunlight. Conditions of intense condensation of moist air penetrating into colder atmospheric environment as a result of thermal flow are favorable for its occurrence. A resonance backscatter effect in delaylines formed by binary collisions of water droplets is consistent with the observations; often, down-looking from aircrafts, bridges, and mountains [http://en.wikipedia.org/wiki/File:Glory_spectre_fogbow_ggb_1.JPG; http://commons.wikimedia.org/wiki/File:IMG_7474_solar_glory.JPG; http://bretwebsterimages.photoshelter.com/image/I0000R.5SZjUbBsg], or emerging from a geyser [http://en.wikipedia.org/wiki/File:Solar_glory_at_the_steam_from_hot_spring.jpg] and barn indoors [http://www.atoptics.co.uk/droplets/gloim9.htm].

According to the resonance model, the sunlight is scattered by coherent interaction with atmospheric microscale aerosol dependent on spectral and spatial parameters. The threshold condition of spectral resonance is established empirically and verified by experimental data on the dispersion of refractive index. The approach is supported by other references demonstrating that the coherence of sunlight exceeds the anticipated limit, e.g., its coherence length as a measure of temporal coherence varies from a few microns to tens of microns when modulated by an interference filter, as well, the spatial coherence as lateral dimension of the interfering rays reaches a few millimeters [*Mashaal et al.,* 2012]. In fact, any interferometric scheme including that of solar glory modulates and changes the coherence characteristics by the well-known uncertainty principle in physics.

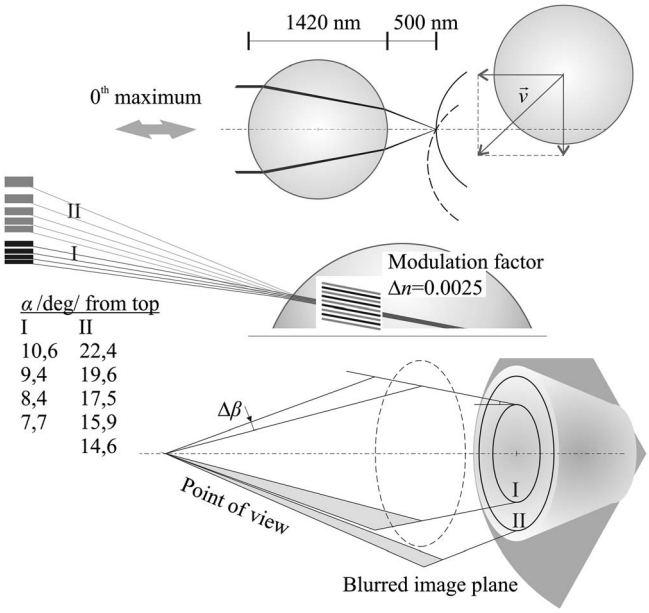

Figure 1. (Top) Ray-diagram of water droplets bound by collision vector *v*; (bottom) spatial characteristics and divergence of the viewing angles of the higher-order diffraction series in the image plane.

2. Resonance Model of Solar Glory

The effect of resonance scattering of sunlight is generated in double-pass delaylines of colliding water droplets within the microscale diffraction limit; it cannot be formed directly in a single-scattering droplet. These optically bound delaylines waveguide and backscatter sunlight analogous to lineups of spherical lenses. The selective spatial and spectral resonance is manifested as backscatter modes of relevant wavelengths and diffraction angles determined by an approach of linear optics. The ray-diagram is viable in the present case tracing the optical paths of constructive and destructive interference of the diffracted light waves. The resonance modes are confined by the gradient of refractive index in concentric circular sectors defined as modal apertures. The resonance optical paths are approximated for a diametric cross section shown on Figure 1.

The ray-diagram is plotted using Snell's law by a fixed gradient of refractive index equal to $\Delta n = 0.00125$, translational and angular resolution equivalent to 1 μm and 5′. The collision vector is not necessarily coaxial with the incident light; as well, the spheres may not be the same size, or touch and diffraction may occur from a large area around the optical axis which increases the probability of scattering.

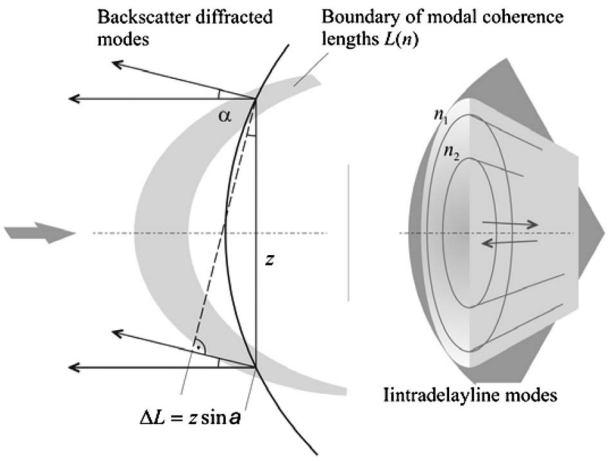

Figure 2. Boundary of modal coherence lengths intersecting the front spherical surface; ΔL is the modulated optical path for derivation of the higher-order diffraction angles.

The central (zero-order) modes are equivalent to normal reflection of the incident light parallel to the optical axis of the delayline. Additional resonance modes are selected by diffraction angles introducing negative gradient $\Delta L = z.\sin\alpha$ to the optical paths on Figure 2. The different diffraction series are similar to those of the diffraction gratings and are numbered further by the same analogy. They share the same resolved resonance optical paths with the central maximum.

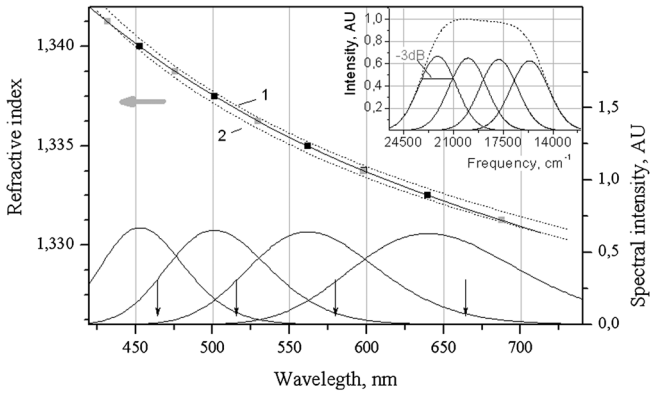

Figure 3. Convolution profile of the central backscatter maximum (first-order marked by arrows); constructive (dark) and destructive (light) data points vs. frequency and wavelength; polynomial-fit (solid line) and experimental dispersions of refractive index of liquid water at 5°C (dotted line 1) and 30°C (dotted line 2).

The first- and second-order diffraction series are observed, thanks to ordinary Mie scattering in the image plane on Figure 1. The spectral contrast of solar glory is blurred increasingly nearer to the optical axis owing to the divergence $\Delta\beta$ of the viewing angle. Better spectral separation is established by the sharp scattering indicatrix of the second-order diffraction series. The central maximum blurred by the same process is close to normal reflection. Its divergence assessed by the second-order diffraction series on pictures taken on the Earth's surface and from space [*Israelevich et al.*, 2009] varies from 3 to 6.5 times the solar angular diameter depending on the remoteness of the observer.

2.1. Modal Coherence Lengths

The resonance condition is expressed by a precise balance established by coincidence or intersection of the virtual boundary of modal coherence lengths with the front surface of the delayline illustrated on Figure 2. The peripheral modes, displaced from the optical axis, correspond to larger wavelengths and experience greater diffraction and defocusing, which induces additional spectral broadening and reduction of modal coherence lengths. The resonance threshold is auto-tuned until it confines the modal coherence lengths exactly within the double-pass intracavity optical paths of the delaylines. Typically, the resonance condition couples selectively a group of adjacent modes matching the dispersion of refractive index.

The modes extend beyond the defined modal apertures and overlap as a result of diffraction. Intermodal destructive interference is prohibited because the separate delaylines are spectrally isolated by the different modal retardations and relevant modal coherence lengths. The gradient of coherence lengths, determined by the curvature of spherical surfaces and variation of modal refractive index, is equal to a modulation factor of a constant value consistent with the presumption of equal conditions of resonance modulation of temporal coherence of adjacent delaylines:

$$\Delta L/L = M = 0.35 \times 10^{-2} \ \ (0.35\ \%) \tag{1}$$

where, $L = \sum \mathrm{l}.n$ is the resonator length equal to the sum of optical paths in the droplet and air.

The modulation factor, as well, corresponds to modal separation by a relevant gradient of refractive index equal to $\Delta n = 0.005$ for solar glory. Exp.1 determines a function of small reduction of the modal coherence lengths across the resonance spectrum:

$$L_p = L_0(1 + M)^p \tag{2}$$

where, p spanning 0–5 represents an arbitrary mode starting from the nearest to the optical axis marked by L_0.

Transient modes in the direction of incident light would always interfere destructively in the focus on the rear surface, i.e., the resonance effect is not observable on the opposite side of the backscattering layer which is consistent with the observations.

Table 1. Parameters of the Central Diffraction Maximum

n	λ, nm	C, AU	ν, cm^{-1}	δ, cm^{-1}	$2L$, nm
1.34	452.8	0.669	22,085	1,848	4,528
1.3375	501	0.651	19,960	1,855	4,509
1.335	561.7	0.64	17,803	1,861	4,493.6
1.3325	639.6	0.628	15,635	1,868	4,477.2

3. Spectral Analysis of Modal Pattern

The resonance modes in a resonance delayline of low finesse are assumed of Gaussian profile. By definition, the modal coherence lengths are reciprocal to their spectral widths (see, e.g., [*Saleh and Teich,* 1991]):

$$\Delta\nu_{FWHM} \approx 0.66/\tau_c, \quad 2L = c\tau_c \approx 0.66 \times c/\Delta\nu_{FWHM} \tag{3}$$

where τ_c is the coherence time and c is the speed of light.

Exp. 4 can be approximated by the definition of coherence length on 0.7 (−3 dB) level of maximal amplitudes used in radio systems:

$$2L = c/f, \quad \text{or} \quad 2L = 1/f, \tag{4}$$

where $f \approx 0.6 \times \Delta\nu_{FWHM}$ is measured in Hz (SI unit) or spectroscopic wave numbers (cm^{-1}).

The optical paths of constructive and destructive interference are described by the following resonance relations of a Fabry-Perot resonator; coefficient m is whole numbers:

$$\text{constructive} : L_m = m \times \lambda/2; \quad \text{destructive} : L_m = (2m+1)\lambda/4 \tag{5}$$

The resonance model explains the observed alternating polarization of the different diffraction series considered previously a puzzling fact. The polarization of the central maximum is typically tangential. Generation of the next first- and second-order modes is possible in two cases that do not interfere with the central modes. Here, the intraresonator optical paths derived by Exp.5 are compensated by a negative gradient introduced by the angular distribution. The first-order modes have radial polarization consistent with the resonance optical paths introducing rotation of the relative phase angle of interfering light waves by $\pi/2$. Consequently, the first-order corresponds to odd numbers of interfering quarter waves:

$$2L_m - \lambda/4 = 2m \times \lambda/2 \rightarrow L_m = (4m+1)8 \quad \text{at} \quad \alpha = \arcsin(\lambda/4z) \tag{6}$$

where the modal displacement z and diffraction angle α are introduced by Figure 2

The second-order series corresponds to odd numbers of half waves, which match the optical paths of destructive interference of the central maximum:

$$2L_m - \lambda/2 = 2m \times \lambda/2 \rightarrow L_m = (2m+1)\lambda/4 \quad \text{at} \quad \alpha = \arcsin(\lambda/2z) \tag{7}$$

The ray-diagram in the previous section allows a relative shift dependent on the distance between droplets which would result in relevant change of the modal parameters. The exact position of the resonance optical paths was determined in successive iterations comparing photographic images with the spectral color scale and circular diameters with the relevant diffraction angles assess by Exp. 6–7. A more precise evaluation is performed by the dispersion of refractive index derived on the basis of the spectral parameters of the central maximum, which is compared to the dispersion of refractive index of liquid water as a function of temperature provided by the International Association of the Properties of Water and Steam (IAPWS). The evaluated spherical size of water droplets and the distance between them are constants, respectively, of 1420

Table 2. Refractive Index of Liquid Water

n	λ, nm	m	n	λ, nm	m
1.34125	432	10	1.335	561.7	8
1.34	452.8	10	1.33375	598	7
1.33875	475.5	9	1.3325	639.6	7
1.3375	501	9	1.33125	687.6	6
1.33625	529.5	8			

Shaded rows correspond to destructive interference.

Table 3. First- and Second-Order Diffraction Series

	n	λ, nm	z, nm	α, deg	m
I	1.339375	464.5	864.4	7.7	–
	1.336875	515.3	876.9	8.4	–
	1.334375	579.7	889	9.4	–
	1.331875	663.7	900.3	10.6	–
II	1.34125	432	854.6	14.6	10
	1.33875	475.5	867.4	15.9	9
	1.33625	529.5	879.7	17.5	8
	1.33375	598	891.7	19.6	7
	1.33125	687.6	903.2	22.4	6

and 500 nm for all diffraction series. A discrepancy of more than five times is established with van de Hulst scattering model of dimensions between 5 and 15 μm [*Laven,* 2005].

3.1. Modal Spectral Widths

The spectral modes are separated on −3 dB level of maximal intensities which results from the intracavity confinement of modal coherence lengths. The resonance fringes overlap uniformly within the interval of free dispersion on the spectral scale as shown on Figure 3. A derivation using Exp.4–5 and assuming $L_{m+1} \simeq L_m$ for adjacent modes proves its validity:

$$D = \nu_m - \nu_{m-1} = m/2L_m - (m-1)/2L_{m+1} = 1/2L = f \tag{8}$$

where D is the free dispersion and f is the −3 dB spectral width.

The modal spectral intensities are proportional to the flux through the modal apertures approximated by the surface of cross sections normal to the optical axis. The resultant resonance spectrum is described by the following convolution sum normalized to unity:

$$\max \sum_m C_m \exp[-(\nu - \nu_m)/\delta_m]^2 = 1 \tag{9}$$

where C, ν, and $\delta = 1/2.\Delta\nu_{\mathrm{FWHM}}$ stand for fringe amplitudes, frequencies, and spectral widths.

The spatial, spectral, and polarization characteristics are summarized in Tables 1–3. The data points approximated by a second-order polynomial on Figure 3 are plotted against IAPWS [http://www.atoptics.co.uk/droplets/gloim9.htm] reference data on dispersion of the refractive index of liquid water. The wavelengths of the first-order series indicated by arrows on the plot are assumed as midpoint values between the resolved optical paths of the ray-diagram instead of using the resonance relations of Exp. 6.

The resonance model is verified by correlation of the simulated and experimental dispersions of the refractive index on Figure 3. The graphical analysis shows that the simulated curve is slightly flatter, which might be caused by insufficient drawing resolution of the ray-diagram if the IAPWS data are assumed utterly correct. The polynomial fit of the evaluated data matches very well the experimental dispersion in the temperature interval 5–30°C though the resolution does not allow determination of the exact temperature of the scattering layer. Nevertheless, the discussed deviation of both profiles that limits the effect of resonance scattering is better outlined.

4. Conclusions

The study resolves a pending problem in atmospheric optics, interpreting the rare spectral phenomenon of solar glory on the basis of resonance scattering of sunlight. According to the developed model, optical interference inside delaylines of colliding microscale water droplets results in a series of backscatter modes via strict balance of temporal coherence preventing destructive intermodal interference. The resonance condition is established for relevant wavelengths in the visible spectrum at selected temperature and spherical size of the scattering droplets. The central modes are equivalent to normal reflection of the incident light. The higher-order modes match the phase difference of interfering light waves introduced by angular divergence. Spectral analysis of the modal pattern is performed by convolution and ray-tracing methods. The derived spectral parameters are verified by the dispersion of refractive index of liquid water compared to accurate experimental data sources.

Acknowledgments

Data supporting Figures 1 and 3 are available as in Supporting Information Tables 1–3.

I thank V. Pencheva and V. Naboko for useful comments encouraging the initial idea.

The editor thanks one anonymous reviewer for their assistance in evaluating this paper.

References

Israelevich, P. L., J. H. Joseph, Z. Levin, and Y. Yair (2009), First Observation of Glory From Space, *Bull. Am. Meteorol. Soc.*, *90*, 1772–1774, doi:10.1175/2009BAMS2824.1.

Laven, P. (2005), Atmospheric glories: Simulations and observations, *Appl. Opt.*, *44*(27), 5667–5674.

Mashaal H., A. Goldstein, D. Feuermann and J.M. Gordon (2012), Spatial coherence of sunlight: first direct measurement, Proc. SPIE 8485, Nonimaging Optics: Efficient Design for Illumination and Solar Concentration IX, 84850A-1-5.

Saleh, B., and M. Teich (1991), *Fundamentals of Photonics*, pp. 351, John Wiley, N. Y.